



HAL
open science

Modeling results on the dust charge distribution in a plasma afterglow

Igor Denysenko, Maxime Mikikian, Nikolai Azarenkov

► **To cite this version:**

Igor Denysenko, Maxime Mikikian, Nikolai Azarenkov. Modeling results on the dust charge distribution in a plasma afterglow. *Physics of Plasmas*, 2022, 29, pp.093702. 10.1063/5.0100913. hal-03780621

HAL Id: hal-03780621

<https://hal.science/hal-03780621v1>

Submitted on 16 Nov 2023

HAL is a multi-disciplinary open access archive for the deposit and dissemination of scientific research documents, whether they are published or not. The documents may come from teaching and research institutions in France or abroad, or from public or private research centers.

L'archive ouverte pluridisciplinaire **HAL**, est destinée au dépôt et à la diffusion de documents scientifiques de niveau recherche, publiés ou non, émanant des établissements d'enseignement et de recherche français ou étrangers, des laboratoires publics ou privés.

Modeling results on the dust charge distribution in a plasma afterglow

Cite as: Phys. Plasmas **29**, 093702 (2022); doi: [10.1063/5.0100913](https://doi.org/10.1063/5.0100913)

Submitted: 27 May 2022 · Accepted: 19 August 2022 ·

Published Online: 20 September 2022



View Online



Export Citation



CrossMark

I. B. Denysenko,^{1,2,3,a)}  M. Mikikian,²  and N. A. Azarenkov^{1,4} 

AFFILIATIONS

¹School of Physics and Technology, V. N. Karazin Kharkiv National University, 61022 Kharkiv, Ukraine

²GREMI, UMR7344 CNRS/Université d'Orléans, F-45067 Orléans, France

³Le Studium, Loire Valley Institute for Advanced Studies, 45000 Orléans, France

⁴National Science Center, Kharkiv Institute of Physics and Technology, 61108 Kharkiv, Ukraine

^{a)} Author to whom correspondence should be addressed: idenysenko@yahoo.com

ABSTRACT

Discharging of dust particles in an argon plasma afterglow is investigated using different approaches. First, the dust charge distribution function (DCDF) is obtained by solving numerically the master equation describing dust discharging as a one-step stochastic process. Second, the DCDF is calculated as a Gaussian distribution with mean dust charge and variance, which are functions of time. Additionally, the time-dependencies for the mean dust charge are obtained assuming that the charge changes continuously in the afterglow plasma. Calculation results are compared with available experimental data and are found to be in good qualitative agreement if the dust discharging model accounts for the emission of electrons in the collisions of excited argon atoms with dust particles. This study is carried out taking into account the transition from ambipolar to free diffusion as well as multistep ionization, excitation, and deexcitation of argon atoms in the plasma afterglow.

Published under an exclusive license by AIP Publishing. <https://doi.org/10.1063/5.0100913>

I. INTRODUCTION

Plasmas with nanosized and micro-sized particles (dust particles) have been extensively studied for several decades.^{1–5} These plasmas (dusty plasmas) are involved in many applications and also in fusion research.^{6–10} They have also been attractive for researchers studying fundamental problems in physics, including the formation of Coulomb dust crystals, dust vortices and voids, wave propagation, cosmic clouds, etc.^{1–4,11,12} Dust charging in steady-state plasmas has also been studied by many authors (see Refs. 1, 2, and 13–15, and references therein) because the dust charge is a key parameter that determines the interaction between a dust particle and electrons, ions, its neighboring dust particles and electric and magnetic fields.

The dust charging phenomenon, or discharging to be more specific, in afterglow plasmas has also been analyzed in many papers.^{16–26} However, in temporary plasma afterglows, most of the authors in their theoretical and numerical studies have used “continuous discharging models,”^{14,27} i.e., the charge on a dust grain is determined by currents collected from the plasma, these currents being continuous in time. Naturally, these models do not account for the discreteness of the dust charge²⁷ and allow to calculate only the mean grain charge. Meantime, due to the discreteness of the charge carriers, the charging process is stochastic and dust charge fluctuations occur.^{27–31}

Stochastic dust charge fluctuations in steady-state plasmas have been studied through various approaches. In particular, Cui and Goree performed Monte Carlo simulations of the dust charging process and demonstrated that small dust particles may briefly exhibit a positive charge.²⁷ Later, it was noted³² that this method in fact solves a master equation, proposed by Matsoukas and Russell,³⁰ to model charging with a one-step stochastic process.²⁹ In Ref. 30, the charging process was described by a Fokker-Planck equation which was obtained by expanding the master equation. It was also found that the charge distribution approaches a Gaussian function with mean charge and variance that bear simple relations to the charging currents.³⁰ In Ref. 33, to describe the charge fluctuations at stationary states, a model utilizing a Langevin equation was developed, and the charge fluctuations were studied for different charging mechanisms, such as thermionic and photoelectric emission. In Refs. 32 and 34, model equations were developed to analyze stochastic charge fluctuations of a dust particle suspended in a plasma at nonstationary states. For this case, it was found that the dust charge distribution function (DCDF) can also be described by a Gaussian distribution, if the size of fluctuations is small compared to the mean charge. However, this approach has not yet been used to calculate the DCDF in an afterglow plasma.

At present, there are only a few works where the DCDF in a temporal afterglow plasma was simulated.^{35,36} These simulations were performed using the Monte Carlo method as in Ref. 27, and taking into account the transition from ambipolar to free diffusion in a decaying plasma. The effects on the dust charge of metastable-dust collisions in the plasma bulk and ion–neutral collisions in the sheath around a dust particle were not taken into account while these collisions may affect essentially the charge.^{17,37}

In this paper, we obtain the DCDF from the master equation describing dust discharging as a one-step stochastic process.^{29–31} An argon plasma afterglow with dust particles is analyzed for the conditions close to those in Refs. 35 and 36 in order to compare the obtained DCDFs. The calculations are carried out accounting for the transition from ambipolar to free diffusion in the plasma afterglow, as in Refs. 35 and 36, and additionally taking into account metastable-dust collisions in the plasma bulk and ion–neutral collisions in the sheath around a dust grain. For different afterglow times, we also compare the DCDFs obtained numerically from the master equation with the Gaussian solutions calculated using the approach proposed in Refs. 32 and 34. The time-dependencies for the mean dust charge and its variance are also obtained.

II. THEORETICAL MODEL

In this section, we first present the model equations describing the evolution of the densities of electrons, ions and excited argon atoms and of the electron temperature in an argon plasma afterglow. Then, we describe the equations used for the analysis of dust particle discharging in the afterglow.

A. Diffusion model of the plasma

Consider an argon low-ionized plasma with radius $R = 2$ cm and height $L = 3$ cm (the plasma sizes here are the same as in Refs. 22, 35, and 36) containing electrons with density n_e , singly charged positive ions (Ar^+) with density n_i , ground-state argon atoms (Ar_0) with density n_a , metastable argon atoms (Ar_m) with density n_m , argon atoms in the resonance 4s states ($^3\text{P}_1$ and $^1\text{P}_1$) (Ar_r) with density n_r as well as argon atoms in 4p states (Ar_{4p}) with density n_{4p} . The metastable and resonance atom densities n_m , n_r , and n_{4p} represent the density of a composite ($^3\text{P}_0$ and $^3\text{P}_2$) metastable level, the density of a composite ($^3\text{P}_1$ and $^1\text{P}_1$) resonance level, and the density of a composite 4p state, respectively. The plasma also contains dust particles with density $n_d = 5 \times 10^4 \text{ cm}^{-3}$, as in Refs. 35 and 36, and radius a_d .

We assume that the ions and dust particles are at gas temperature T_g ($= 0.026$ eV), and the ions and electrons have Maxwellian distributions. The calculations are carried out for neutral gas pressures $P = 0.3$ and $P = 0.9$ Torr, as in Refs. 35 and 36.

The time-dependencies for the electron and ion densities are described, respectively, by the following balance equations:

$$\frac{\partial n_e}{\partial t} = K^{R1} n_a n_e + K^{R2} n_m^2 + K^{R3} n_m n_e + K^{R4} n_r n_e + K^{R5} n_{4p} n_e + K^{R6} n_m n_r + K^{R7} n_{4p}^2 - R_{we} n_e - K_e^d n_e n_d + \gamma_m K_m^d n_d (n_m + n_r + n_{4p}), \quad (1)$$

$$\frac{\partial n_i}{\partial t} = K^{R1} n_a n_e + K^{R2} n_m^2 + K^{R3} n_m n_e + K^{R4} n_r n_e + K^{R5} n_{4p} n_e + K^{R6} n_m n_r + K^{R7} n_{4p}^2 - R_{wi} n_i - K_i^d n_i n_d, \quad (2)$$

TABLE I. Production and loss processes of electrons and ions taken into account in the model. Here, Ar^* corresponds to the argon atom in an excited state.

Reaction	Rate	References
(R1) $e + \text{Ar}_0 \rightarrow \text{Ar}^+ + 2e$	$K^{R1} = f(\sigma)$	38
(R2) $\text{Ar}_m + \text{Ar}_m \rightarrow \text{Ar} + \text{Ar}^+ + e$	$K^{R2} = 1.24 \times 10^{-10} \text{ cm}^3/\text{s}$	25
(R3) $e + \text{Ar}_m \rightarrow \text{Ar}^+ + 2e$	$K^{R3} = f(\sigma)$	39
(R4) $e + \text{Ar}_r \rightarrow \text{Ar}^+ + 2e$	$K^{R4} = f(\sigma)$	39
(R5) $e + \text{Ar}(4p) \rightarrow \text{Ar}^+ + 2e$	$K^{R5} = f(\sigma)$	40
(R6) $\text{Ar}_m + \text{Ar}_r \rightarrow \text{Ar} + \text{Ar}^+ + e$	$K^{R6} = 2.1 \times 10^{-9} \text{ cm}^3/\text{s}$	41
(R7) $\text{Ar}(4p) + \text{Ar}(4p) \rightarrow \text{Ar}^+ + \text{Ar} + e$	$K^{R7} = 5.0 \times 10^{-10} \text{ cm}^3/\text{s}$	41
(R8) $e \rightarrow \text{wall}$	$R_{we} = D_e/\Lambda^2$	42–45
(R9) $e + \text{dust}(Z_d) \rightarrow \text{dust}(Z_d - 1)$	K_e^d	1, 2
(R10) $\text{dust}(Z_d) + \text{Ar}^* \rightarrow \text{dust}(Z_d + \gamma_m) + \gamma_m e + \text{Ar}_0$	K_m^d	17
(R11) $\text{Ar}^+ \rightarrow \text{wall}$	$R_{wi} = D_i/\Lambda^2$	42
(R12) $\text{Ar}^+ + \text{dust}(Z_d) \rightarrow \text{dust}(Z_d + 1)$	K_i^d	17, 37

where t is the afterglow time, and K^{Ri} is the rate for a reaction accompanied by production/loss of electrons or ions. The corresponding reactions are shown in Table I.

The rate coefficients for reactions (R1) and (R3)–(R5) are calculated using the corresponding reaction cross sections σ taken from Refs. 38–40 and assuming that the electron energy distribution function (EEDF) is Maxwellian. $\Lambda = 1/\sqrt{(\pi/L)^2 + (2.405/R)^2}$ is the diffusion length. D_e and D_i are the diffusion coefficients for electrons and ions, respectively. In the steady-state ($t = 0$), it is assumed that $D_e = D_i = D_a$, where $D_a \approx D_{if}(1 + T_e/T_i)$ is the ambipolar diffusion coefficient. T_e and T_i are the electron and ion temperatures, respectively. $D_{if} \approx \lambda_i v_i/3$ is the ion free diffusion coefficient, where $v_i = \sqrt{8eT_i/\pi m_i}$ is the ion thermal velocity, m_i is the ion mass, $\lambda_i = 1/(n_a \sigma_{ia})$ is the ion mean-free path, and $\sigma_{ia} \approx 10^{-14} \text{ cm}^2$ is the cross section for ion–neutral collisions. Our model takes into account the transition from ambipolar to free diffusion in the afterglow plasma. It is assumed that $D_i = D_{if} + (1.5D_a - D_{if})[1.0 - \exp\{-\Lambda^2/(4.5\lambda_{De}^2)\}]$ for $\Lambda^2/\lambda_{De}^2 < 150$, $D_i = 1.5 \times D_a \left\{ \frac{1}{2} \left[\frac{\Lambda^2/\lambda_{De}^2 - 150}{3000 - 150} \right]^{0.4} + 1 \right\}$ for $150 \leq \Lambda^2/\lambda_{De}^2 < 3000$ and $D_i = D_a$ for $\Lambda^2/\lambda_{De}^2 \geq 3000$ (solid curve in Fig. 1), where λ_{De} is the electron Debye length. The dependence of D_i on Λ/λ_{De} approximates well the measured dependence in Ref. 42 in the case $T_e = T_i$. For electrons, it is assumed that the diffusion coefficient D_e is connected with the ambipolar diffusion coefficient as in Ref. 43 for the fast transition case (dashed curve in Fig. 1) or is described by empirical formulas (40) and (41) in Ref. 44, which were initially obtained in Ref. 45, for the slow transition case (dotted curve in Fig. 1). The formulas (40) and (41) in Ref. 44 describe well the measured dependence of D_e on Λ/λ_{De} in Ref. 42.

The rate coefficients for reactions (R9) and (R12) are $K_e^d = \sum_k F_k \nu_{ed}^k/n_e$ and $K_i^d = \sum_k F_k \nu_{id}^k/n_i$, respectively, where F_k is

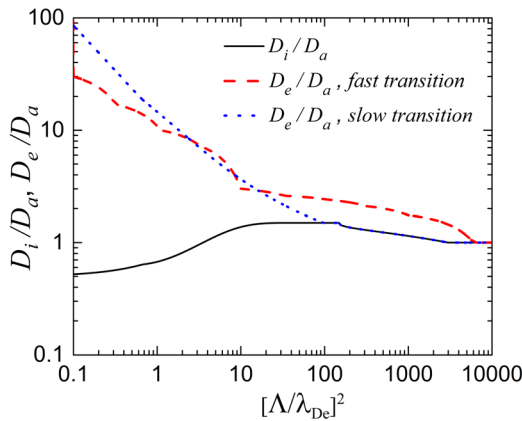


FIG. 1. D_i/D_a and D_e/D_a as functions of $(\Lambda/\lambda_{De})^2$ used in present model. The solid curve corresponds to D_i/D_a , while the dashed and dotted curves describe D_e/D_a obtained using experimental results of Freiberger and Weaver⁴⁵ (fast transition case) and empirical formulas⁴⁴ (slow transition case), respectively.

the dust charge distribution function, and ν_{ed}^k and ν_{id}^k are the frequencies with which a particle with charge $Z_d^k = ke$ collects electrons and ions, respectively. k is an integer, and the DCDF is normalized by $\sum_k F_k = 1$. The expressions for ν_{ed}^k and ν_{id}^k are presented in Section II B.

The model also assumes that electrons can be generated due to electron emission from the dust surface due to collisions with argon atoms in excited states. The process is described by reaction (R10) and is characterized by the yield γ_m and the rate $K_m^d = \pi a_d^2 \sqrt{8eT_g/\pi m_i}$.

The model also includes the balance equations for argon atoms in different excited states, which can be presented in the following form:

$$\frac{\partial n^{(X)}}{\partial t} = \sum_i R_{G,i}^{(X)} - \sum_i R_{L,i}^{(X)}, \quad (3)$$

where $n^{(X)}$ is n_m , n_r , or n_{4p} , $R_{G,i}^{(X)}$ and $R_{L,i}^{(X)}$ are, respectively, the rates for reactions of the various generation and loss processes of the species with density $n^{(X)}$. The reactions taken into account to calculate the metastable, 4s resonant, and 4p atoms densities are shown in Tables I and II, and described in detail in Ref. 25. The rate coefficients for reactions (R13)–(R16), (R18), and (R20)–(R22) are calculated using the corresponding reaction cross sections σ taken from Refs. 46–48, and assuming that the EEDF is Maxwellian. In Table II, $D_m \approx 2.42 \times 10^{18}/n_a$ (where n_a in cm^{-3}) is the metastable diffusion coefficient.⁴⁸ It is assumed that $K^{R17} = 2 \times 10^{-7} \text{ cm}^3/\text{s}$ for the power on phase⁴⁸ and is in 5 times smaller in the afterglow.²⁵

The time evolution of electron temperature in the plasma afterglow can be found from the following power balance equation:

$$\frac{\partial}{\partial t} \left(\frac{3}{2} n_e T_e \right) = \frac{(P_{\text{abs}} - P_{\text{loss}})}{V}, \quad (4)$$

where P_{abs} is the power absorbed in the plasma volume in the power on phase ($t = 0$) and $P_{\text{loss}} \approx P_w + P_{\text{coll}}$. In our calculations, the power P_{abs} is chosen to have $n_e(t = 0) = 5.0 \times 10^9 \text{ cm}^{-3}$, as in Ref. 36.

In the plasma afterglow, $P_{\text{abs}} = 0$. The power loss on the walls is $P_w = eV(n_i D_i \varepsilon_i + n_e D_e \varepsilon_e)/\Lambda^2$, where $\varepsilon_i \approx 5.2T_e$ and $\varepsilon_e = 2T_e$ are the mean kinetic energy lost respectively per ion and electron.⁵⁰

TABLE II. Production and loss processes of excited argon atoms taken into account in the model, additionally to those in Table I.

Reaction	Rate	References
(R13) $e + \text{Ar}_0 \rightarrow \text{Ar}_m + e$	$K^{R13} = f(\sigma)$	46
(R14) $e + \text{Ar}_0 \rightarrow \text{Ar}_r + e$	$K^{R14} = f(\sigma)$	46
(R15) $e + \text{Ar}_0 \rightarrow \text{Ar}(4p) + e$	$K^{R15} = f(\sigma)$	46
(R16) $e + \text{Ar}_m \rightarrow \text{Ar}(4p) + e$	$K^{R16} = f(\sigma)$	47
(R17) $e + \text{Ar}_m \rightarrow \text{Ar}_r + e$	K^{R17}	25,48
(R18) $e + \text{Ar}_r \rightarrow \text{Ar}(4p) + e$	$K^{R18} = f(\sigma)$	47
(R19) $e + \text{Ar}_r \rightarrow \text{Ar}_m + e$	$K^{R19} = 9.1 \times 10^{-7} \text{ cm}^3/\text{s}$	41
(R20) $e + \text{Ar}_m \rightarrow \text{Ar}_0 + e$	$K^{R20} = f(\sigma)$	46, 49 ^a
(R21) $e + \text{Ar}_r \rightarrow \text{Ar}_0 + e$	$K^{R21} = f(\sigma)$	46, 49 ^a
(R22) $e + \text{Ar}(4p) \rightarrow \text{Ar}_0 + e$	$K^{R22} = f(\sigma)$	46, 49 ^a
(R23) $\text{Ar}_0 + \text{Ar}_m \rightarrow \text{Ar}_0 + \text{Ar}_0$	$2.1 \times 10^{-15} \text{ cm}^3/\text{s}$	41
(R24) $\text{Ar}_r \rightarrow \text{Ar} + \hbar\omega$	10^5 s^{-1}	41
(R25) $\text{Ar}(4p) \rightarrow \text{Ar} + \hbar\omega$	$3.2 \times 10^7 \text{ s}^{-1}$	41
(R26) $\text{Ar}(4p) \rightarrow \text{Ar}_m + \hbar\omega$	$3.0 \times 10^7 \text{ s}^{-1}$	41
(R27) $\text{Ar}(4p) \rightarrow \text{Ar}_r + \hbar\omega$	$3.0 \times 10^7 \text{ s}^{-1}$	41
(R28) $\text{Ar}_m (\text{Ar}_r) \rightarrow \text{Ar}_0 (\text{wall})$	D_m/Λ^2	48

^aObtained by applying the principle of detailed balancing to the cross section given in the cited reference.

$$P_{\text{coll}} = en_e V \left\{ \sum_X n^{(X)} \left(\sum_i \varepsilon_{ex,i}^{(X)} K_{ex,i}^{(X)} - \sum_k \varepsilon_{dex,k}^{(X)} K_{dex,k}^{(X)} \right) + n_a (3m_e/m_a) K_{ea} (T_e - T_g) \right\},$$

where $K_{ex,i}^{(X)}$ and $\varepsilon_{ex,i}^{(X)}$ are, respectively, the rate coefficient and electron energy loss at excitation (or ionization) of species $n^{(X)}$ by electron impact for the reactions (R1), (R3)–(R5), and (R13)–(R18) in Tables I and II. $K_{dex,k}^{(X)}$ and $\varepsilon_{dex,k}^{(X)}$ are, respectively, the rate coefficient and the electron energy gain at deexcitation of species $n^{(X)}$ by electron impact for the reactions (R19)–(R22). K_{ea} is the rate for electron-atom momentum transfer collisions, which was obtained using the corresponding cross section in Ref. 38. Since the dust charge density is assumed to be low compared with the electron density ($|n_d \sum_k F_k Z_d^k| \ll n_e$) during most of the time when the electron temperature drops in the afterglow, the energy loss on dust particles is not taken into account in Eq. (4). Additionally, we assume that the electron temperature cannot be smaller than the gas temperature in the afterglow.

Note that we obtain the time-dependence for electron temperature taking into account for multistep ionization and excitation and deexcitation of argon atoms by electron impact. Meantime, in our previous studies,^{17,25} to describe the electron temperature variation in argon/dust pulsed and afterglow plasmas, these processes were not taken into account. However, in Refs. 51–53, it was shown that multistep ionization and excitation and deexcitation of argon atoms by electron impact may affect essentially the time-dependence for electron temperature in afterglow plasmas. Our calculations confirmed this conclusion (see the supplementary material). Moreover, it was found that considering the effect of multistep ionization and excitation and deexcitation of argon atoms gives a DCDF and mean dust charge at

late afterglow times, which are different from those obtained using the model that does not account for this effect (the results obtained using the simplified model are presented in [supplementary material](#)).

B. Discharging of dust particles in the plasma afterglow

Here, we assume that dust particles of the same radius a_d may have different charges due to stochastic charge fluctuations connected with charge discreteness. The charges of dust particles are characterized by the DCDF F_k , which can be described by the following master equation for the one-step process:^{30–32}

$$\frac{d}{dt}F_k = \nu_{ed}^{k+1}F_{k+1} - \nu_{ed}^kF_k - (\nu_{id}^k + \nu_m)F_k + (\nu_{id}^{k-1} + \nu_m)F_{k-1}, \quad (5)$$

where for $Z_d^k < 0$, $\nu_{id}^k \approx n_i a_d^2 \sqrt{8\pi e T_i / m_i} (1 - \zeta_k \tau + H_k \zeta_k^2 \tau^2 \lambda_s n_a \sigma_{ia})$, $\zeta_k = \varphi_{sk} / T_e$, $\tau = T_e / T_i$, $\nu_{ed}^k = n_e a_d^2 \sqrt{8\pi e T_e / m_e} \exp(\varphi_{sk} / T_e)$, m_e is the electron mass, and $\varphi_{sk} = e Z_d^k / a_d$. Here, $H_k \sim 0.1$ for $0.1 \leq \beta \leq 10$, $H_k \sim \beta$ for $\beta < 0.1$, and $H_k \sim \beta^{-2} (\ln \beta)^3$ for $\beta \gg 1$,³⁷ where $\beta = |e Z_d^k| / \lambda_s T_i$, and λ_s is the screening length, which is of the same order as the Debye length.⁶ In the expression for ν_{id}^k , ion–neutral collisions in the sheath around a dust particle are accounted for. The terms in the right-hand side of Eq. (5), which are proportional to $\nu_m = \gamma_m K_m^d (n_m + n_r + n_{4p})$, account for electron emission from the dust surface at collisions of dust particles with argon atoms in excited states.

For $Z_d^k > 0$, $\nu_{ed}^k = n_e a_d^2 \sqrt{8\pi e T_e / m_e} (1 + \varphi_{sk} / T_e)$ and $\nu_{id}^k \approx n_i a_d^2 \sqrt{8\pi e T_i / m_i} \exp(-\varphi_{sk} / T_i)$.

We also calculate the mean dust charge Z_d using the following expression:

$$\frac{\partial Z_d}{\partial t} = \nu_{id} + \gamma_m K_m^d (n_m + n_r + n_{4p}) - \nu_{ed}, \quad (6)$$

where ν_{id} and ν_{ed} are coinciding with the corresponding expressions for ν_{id}^k and ν_{ed}^k if one replaces in these expressions Z_d^k by Z_d . Here, we consider the cases when the mean dust charge is negative.

We also compare the DCDF calculated from Eq. (5) with the Gaussian distribution,^{32,34}

$$F_{Gk} = \frac{1}{(2\pi\sigma_z^2)^{1/2}} \exp\left[-\frac{(-Z_d^k + Z_d)^2}{2\sigma_z^2}\right], \quad (7)$$

where Z_d is determined by Eq. (6), and the variance σ_z^2 as a function of time is found from the following equation:^{32,34}

$$\frac{d\sigma_z^2}{dt} \approx -\alpha_1' \sigma_z^2 + \alpha_2, \quad (8)$$

where $\alpha_1' = 2(\nu_{ed}' - \nu_{id}')$ with primes indicating derivatives with respect to Z_d , $\alpha_2 = \nu_{ed} + \nu_{id} + \gamma_m K_m^d (n_m + n_r + n_{4p})$. In a steady-state plasma ($t = 0$) and when $\gamma_m = 0$, $\sigma_z^2 \approx \frac{\nu_{ed} + \nu_{id}}{2(\nu_{ed}' - \nu_{id}')$.^{30,31} Note that the expressions for σ_z^2 can be used only if $\nu \gg \nu' \gg \nu''$ for both the electron and ion flux.^{30,31}

The equations for each particle (electrons, ions, excited argon atoms in metastable and 4s and 4p resonance states), the power balance equation (4), the equation for mean dust charge (6), and the system of equations for DCDF following from Eq. (5) are solved

numerically by using the DVODE package.⁵⁴ The initial values of plasma parameters, except $n_e(0)$ and $n_i(0)$, are obtained setting $\partial/\partial t = 0$ in the model equations. It is assumed that at $t = 0$, $n_e = n_i = 5 \times 10^9 \text{ cm}^{-3}$, as in Ref. 36.

III. RESULTS

Using the equations presented in Sec. II, we have calculated the electron, ion and metastable atom densities, electron temperature, mean dust charge Z_d , and dust charge distribution function F_k for different afterglow times. The numerical calculations have been carried out for the conditions typical to experiments on argon/dust afterglow plasmas^{22,35,36} in the PKE-Nefedov reactor⁵⁵ for $P = 0.3$ and $P = 0.9$ Torr. In this section, the charges Z_{dmax}^k corresponding to the maximum of F_k and the dust distribution functions are compared with the mean charges Z_d and the Gaussian distributions F_{Gk} , respectively. We also compare the calculated F_k with the measured charge distributions presented in Ref. 36. The results are obtained taking into account secondary electron emission in the collisions of excited argon atoms Ar^* (Ar_m , Ar_r , and Ar_{4p}) with dust particles [(R10) in Table I] for different values of γ_m , as well as neglecting this process ($\gamma_m = 0$). Since the values of γ_m are not known for the conditions considered here, we use in our simulations the values leading to a good agreement with experimental data.^{35,36} The calculations have been carried out for the cases of fast and slow transition in the decaying plasma.

A. The fast transition case

First, consider the case of fast transition at $P = 0.3$ Torr. For this case, the mean dust charge as a function of time is shown for $\gamma_m = 0$ and $\gamma_m = 0.035$ in Fig. 2(a). In this figure, the time-dependencies for the charge Z_{dmax}^k corresponding to the maximum of F_k are also presented. The electron temperature and metastable atom density as functions of time for the $\gamma_m = 0$ case are shown in Fig. 2(b), while the time-dependencies for n_e and n_i are presented in Fig. 2(c). The time-dependencies for T_e , n_m , n_s , and n_i obtained at $\gamma_m = 0.035$ are not shown here because they were found to be nearly the same as those for the case when $\gamma_m = 0$.

One can see in Fig. 2(a) that discharging of dust particles in the plasma afterglow can be divided in several phases. During phase I, which starts at $t = 0$ and ends at $t \approx 0.1$ ms, the amount of negative charge on the dust particles decreases rapidly because the frequency describing deposition of ions on a dust particle (ν_{id}) is larger than that of electrons due to rapid decrease in the electron temperature [Fig. 2(b)]. In this phase, the decrease in T_e is mainly due to electron energy loss in collisions with argon atoms in the ground state and due to diffusion of electrons and ions to the walls; multistep ionization and excitation and deexcitation of argon atoms by electron impact do not affect essentially the time-dependence for electron temperature (see the [supplementary material](#)). During phase II [at $0.1 \text{ ms} \leq t \leq 15 \text{ ms}$ in Fig. 2(a)], $|Z_d|$ also decreases with increasing time. However, the decrease is not only due to decreasing of the electron temperature (at $t \leq 5 \text{ ms}$), but also due to larger n_i compared with n_e (at $t > 1 \text{ ms}$) [Fig. 2(c)], and due to metastable-dust collisions (at $t > 2 \text{ ms}$ in the $\gamma_m = 0.035$ case). Meantime, in the $\gamma_m = 0$ case, the decrease in $|Z_d|$ in phase II is not so fast as in phase I because of slower variation of T_e in phase II.

At $t \approx 2 \text{ ms}$, n_i and n_e are significantly less than the corresponding initial densities [Fig. 2(c)], while the decrease in n_m during the first

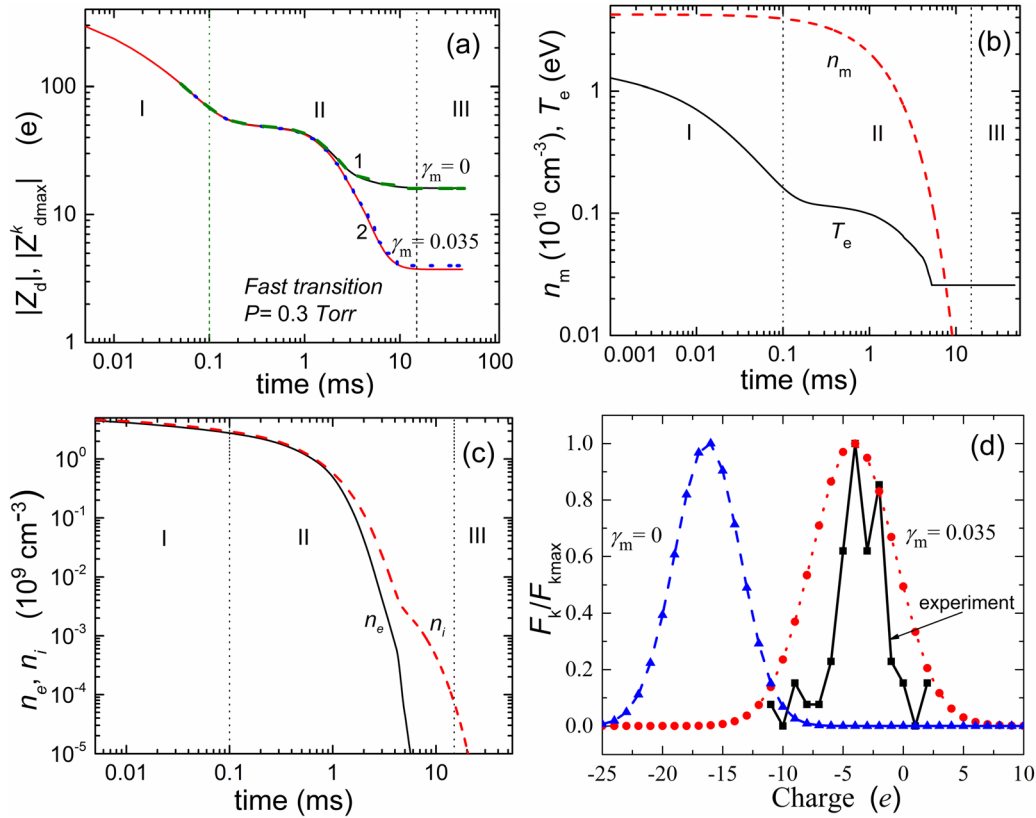


FIG. 2. (a) The mean dust charge (curves 1 and 2) and Z_{dmax}^k (dashed and dotted curves) as functions of time. The curve 1 and the dashed curve are calculated for the $\gamma_m = 0$ case. The curve 2 and the dotted curve are obtained at $\gamma_m = 0.035$. (b) The time-dependencies for electron temperature and n_m . (c) The electron and ion densities as functions of time. (d) The normalized DCDFs calculated for the $\gamma_m = 0$ case (dashed curve) and $\gamma_m = 0.035$ (dotted curve); and the DCDF obtained in experiments³⁶ (solid curve). Here, $F_{kmax} = F_k(Z_{dmax}^k)$ and the results are calculated for the case of fast transition at $P = 0.3$ Torr and $a_d = 190$ nm.

two milliseconds is not so large [Fig. 2(b)]. As a result, for $t > 2$ ms, discharging of dust particles due to their collisions with metastable argon atoms may become essential, and $|Z_d|$ calculated with $\gamma_m = 0.035$ becomes smaller than with $\gamma_m = 0$ [Fig. 2(a)]. Note that for $t < 2$ ms, discharging of dust particles in their collisions with metastable atoms [Fig. 2(a)] is not essential (curves 1 and 2 are nearly superimposed) because the frequency for ion–dust collisions is larger than that describing the secondary emission process [$\nu_{id} > \gamma_m K_m^d (n_m + n_r + n_{4p})$].

During phase III, when $t > 15$ ms, the dust charge becomes time-independent because the frequencies describing deposition of plasma species on a dust grain are very small due to vanishing n_m , n_e and n_i [Figs. 2(b) and 2(c)].

Using Eq. (5), we have calculated the normalized DCDFs in the late afterglow (here, for $t = 50$ ms). In Fig. 2(d), the calculated DCDF agrees well with the one obtained in experiments,³⁶ if our model accounts for the increase in energy of electrons due to their collisions with argon atoms in different excited states and for the secondary emission with $\gamma_m = 0.035$ [Fig. 2(d)]. Note also that the time-dependence for mean dust charge obtained from Eq. (6) is nearly the same as for the charge Z_{dmax}^k corresponding to the DCDF maximum [Fig. 2(a)].

The charge distributions calculated from Eq. (5) in the $\gamma_m = 0.035$ case have been compared with the Gaussian distributions

obtained using Eqs. (7) and (8) for different afterglow times. It has been found that the Gaussian distributions approximate well the DCDFs [Figs. 3(a)–3(c)] even if the deviation increases at large afterglow times [Fig. 3(c)], when σ_z has nearly the same magnitude as the mean dust charge [Figs. 2(a) and 3(d)]. Note that the Gaussian solution was obtained assuming that the size of fluctuations is small compared to the mean charge.^{29,32,34}

Figure 3(d) shows the time-dependencies for the variance of the dust charge. The variance decreases with time until $t \leq 3$ ms and increases at $4 \text{ ms} < t \leq 8$ ms. In our opinion, this increase in σ_z^2 in the $\gamma_m = 0$ case is mainly due to decreasing the ratio of ν_{ed}/ν_{id} (because of the transition from ambipolar to free diffusion in the plasma afterglow). To check this conclusion, we have analyzed the expression for variance in the case of steady-state plasma³¹ ($\sigma_z^2 \approx \frac{\nu_{ed} + \nu_{id}}{2(\nu_{ed} - \nu_{id})}$).

OML approximation, the last expression can be written in the following form: $\sigma_z^2 \approx \frac{(1 + \nu_{ed}/\nu_{id}) a_d T_e}{2e(\tau/(1 + \tau|z|) + \nu_{ed}/\nu_{id})}$, where $z = eZ_d/a_d T_e$. When $\tau/(1 + \tau|z|) < 1$, a decrease in ν_{ed}/ν_{id} affects more essentially the denominator of expression for σ_z^2 than its numerator. As a result, a decrease in ν_{ed}/ν_{id} may be accompanied by increasing σ_z^2 . It also follows from the expression for σ_z^2 that at late afterglow times, when τ and z are time-independent and $\nu_{ed}/\nu_{id} \approx 0$, the variance is also

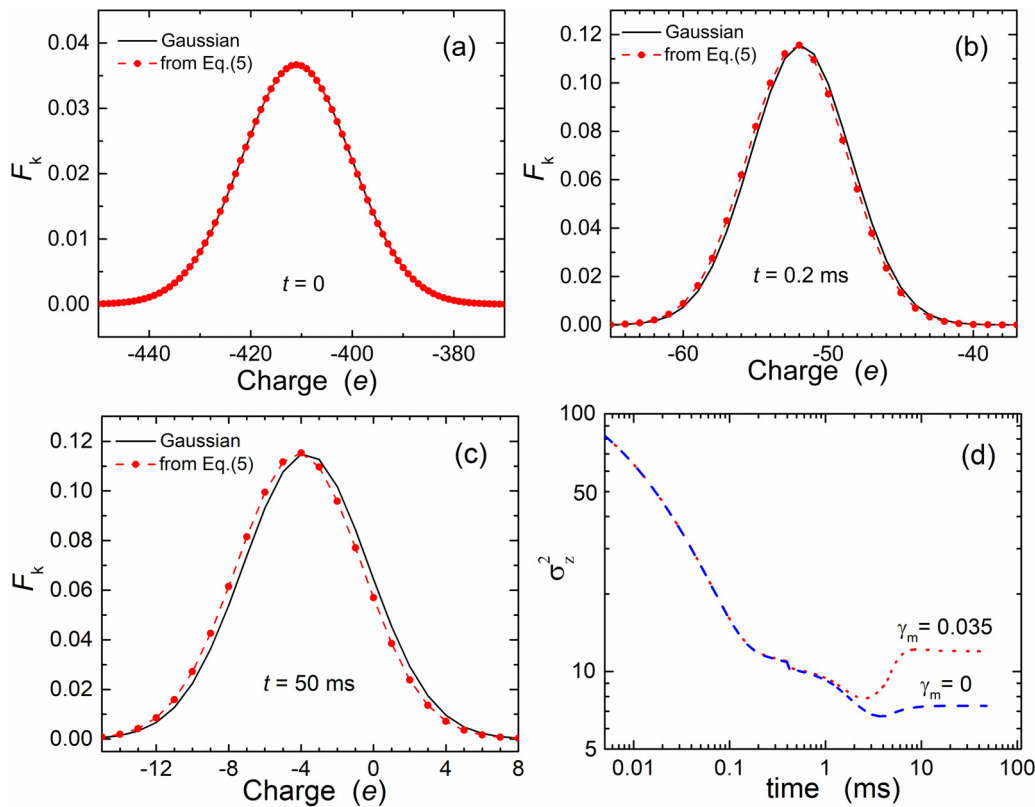


FIG. 3. The DCDFs obtained from Eq. (5) (dashed curves with circles) and the Gaussian distribution functions obtained from Eq. (7) (solid curves) for the $\gamma_m = 0.035$ case at $t = 0$ (a), $t = 0.2$ ms (b), and $t = 50$ ms (c). The variance as a function of time (d) for the $\gamma_m = 0$ (dashed curve) and $\gamma_m = 0.035$ (dotted curve) cases. The other conditions are the same as in Fig. 2.

time-independent, in good agreement with the dependences in Fig. 3(d). If $\gamma_m \neq 0$, the variance for the steady-state case is $\sigma_z^2 \approx \frac{\nu_{ed} + \nu_{id} + \gamma_m K_m^d (n_m + n_r + n_{ap})}{2(\nu_{ed} - \nu_{id})}$, i.e., it is increasing with an increase in γ_m , also in good agreement with the dependences in Fig. 3(d). Note that for the steady-state case, usually⁵⁰ $\sigma_z \approx 0.5\sqrt{|Z_d|}$. In our case, $\sigma_z = 0.54\sqrt{|Z_d|}$ for $t = 0$.

Next, consider the case when $P = 0.9$ Torr. For this case, the electron and ion densities, and the electron temperature as functions of time in the plasma afterglow are shown in Fig. 4(a).

The dependencies presented in Fig. 4(a) are similar to those in Fig. 2. However, n_e , n_i , and T_e decrease more slowly with increasing t at $P = 0.9$ Torr because of less-intensive diffusion of ions and electrons to the walls (smaller ion and electron mean-free paths because of larger ion-neutral and electron-neutral collision frequencies). The initial electron temperature at $P = 0.9$ Torr ($T_e = 1.39$ eV) is smaller than at $P = 0.3$ Torr ($T_e = 1.71$ eV) also due to smaller losses of ions and electrons on the walls (smaller ambipolar diffusion coefficient). Because of smaller initial electron temperature, the initial metastable density at $P = 0.9$ Torr ($n_m = 3.0 \times 10^{10} \text{ cm}^{-3}$) is smaller than at $P = 0.3$ Torr ($n_m = 4.2 \times 10^{10} \text{ cm}^{-3}$). At $t = 0$, $|Z_d| = 284$ and 411 for 0.9 and 0.3 Torr, correspondingly, i.e., the initial absolute value of dust charge decreases with increasing pressure, mainly due to the enhancement of ion-neutral collisions around dust particles.³⁷

For $P = 0.9$ Torr, similarly to the $P = 0.3$ Torr case [Fig. 2(a)], the time-dependence for the mean dust charge and $Z_{d\text{max}}^k$ has been found to be nearly the same (not shown here).

For $P = 0.9$ Torr and late afterglow times, the dust charge distribution function calculated from Eq. (5) agrees well with the measured one, if the secondary emission yield is 0.01 [Fig. 4(b)]. If $\gamma_m = 0$, the calculated DCDF is shifted to smaller charge values as at 0.3 Torr [Fig. 2(d)].

At $P = 0.9$ Torr, the DCDF calculated from the master Eq. (5) can be well described by the Gaussian distribution [Fig. 4(b)] with the variance determined by Eq. (8), this agreement being better than at $P = 0.3$ Torr [Figs. 3(c) and 4(b)]. It has also been found that the time-dependencies for variance at $P = 0.9$ Torr are similar to those for the $P = 0.3$ Torr case [Fig. 3(d)].

B. The slow transition case

We have also considered the case when the transition from ambipolar to free diffusion takes place at rather small $\Lambda^2/\lambda_{De}^2 (\leq 100)$ (the slow transition case). The mean dust charge, electron, ion and metastable atom densities and T_e as functions of time in the plasma afterglow are presented in Figs. 5(a)–5(c), first for $P = 0.3$ Torr.

One can see in Fig. 5(b) that the time-dependencies for T_e and n_m are nearly the same as in the fast transition case [Fig. 2(b)]. However, the difference between n_e and n_i in the slow transition case

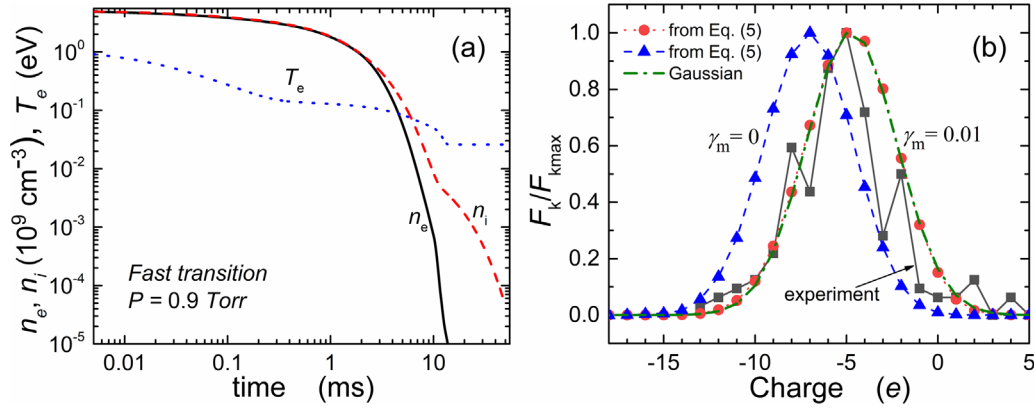


FIG. 4. n_e (solid curve), n_i (dashed curve), and T_e (dotted curve) as functions of time (a). The normalized dust charge distribution functions calculated from Eq. (5) in the late afterglow for $\gamma_m = 0$ (dashed curve) and 0.01 (dotted curve with circles), and the normalized DCDF obtained in experiments³⁶ (solid curve) (b). The dash-dotted curve corresponds to the normalized Gaussian distribution obtained from Eq. (7) at $\gamma_m = 0.01$. Here, $P = 0.9$ Torr and the other conditions are the same as in Fig. 2.

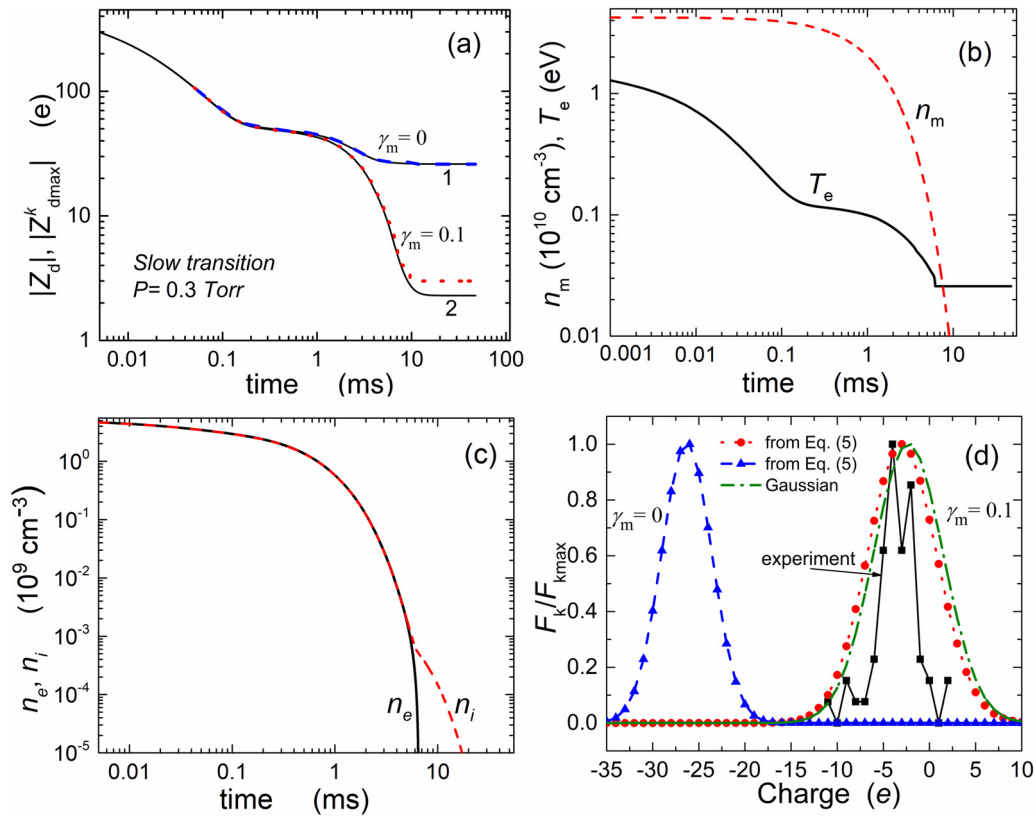


FIG. 5. The mean dust charge (curves 1 and 2) and Z_{dmax}^k (dashed and dotted curves) as functions of time (a). The curve 1 and dashed curve are for $\gamma_m = 0$, and the curve 2 and dotted curve —for $\gamma_m = 0.1$. The time-dependencies for electron temperature and n_m (b). n_e and n_i as functions of time (c). The normalized dust charge distribution functions calculated from Eq. (5) in the late afterglow for $\gamma_m = 0$ (dashed curve) and 0.1 (dotted curve), and the normalized DCDF obtained in experiments³⁶ (solid curve) (d). The dash-dotted curve in Fig. 5(d) corresponds to the normalized Gaussian distribution at $\gamma_m = 0.1$. The dependencies are obtained for the slow transition case and $P = 0.3$ Torr. The other conditions are the same as in Fig. 4.

becomes essential only when $n_e \leq 10^6 \text{ cm}^{-3}$, while the difference for the fast transition is observed at $n_e \leq 10^8 \text{ cm}^{-3}$ [Fig. 2(c)]. Because of this difference, the decrease in $|Z_d|$ in the afterglow plasma at $\gamma_m = 0$ in the slow transition case is not so large as in the fast transition case [curves 1 in Figs. 2(a) and 5(a)]. As a result, the DCDF calculated for $\gamma_m = 0$ and late afterglow times in the slow transition case differs more essentially from the measured one than in the fast transition case [Figs. 2(d) and 5(d)]. Indeed, at late afterglow times ($t \geq 50 \text{ ms}$), $Z_{d\text{max}}^k = -26$ and -16 for the low and fast transition cases, respectively, while in the experiment the maximum of DCDF is observed at $Z_d = -4$.

A good agreement between the calculated DCDFs from Eq. (5) and measured DCDFs can be obtained, if the model accounts for the secondary electron emission in the collisions of excited argon atoms with dust particles [Figs. 2(d) and 5(d)]. Meantime, the secondary emission yield γ_m in the slow transition case is found to be larger (here, for $P = 0.3 \text{ Torr}$, $\gamma_m = 0.1$) than the one in the fast transition case ($\gamma_m = 0.035$). For $P = 0.3 \text{ Torr}$, $\gamma_m = 0.1$ and late afterglow times, the Gaussian distribution obtained from Eq. (7) is slightly different from the DCDF calculated from Eq. (5) [Fig. 5(d)].

Note that similarly to the fast transition case [Fig. 2(a)], the dependencies for Z_d and Z_d^k also agree well in the slow transition case [Fig. 5(a)]. The time-dependencies for σ_z^2 obtained in the slow transition case for $\gamma_m = 0$ and $\gamma_m = 0.1$ have been found (not shown here) to be similar to the corresponding dependencies obtained in the fast transition case [Fig. 3(d)].

Considering the slow transition case, we have also analyzed the afterglow plasma when $P = 0.9 \text{ Torr}$. It has been found that the DCDF obtained from Eq. (5) agrees well with the measured distribution if $\gamma_m = 0.1$ (similar to the $P = 0.3 \text{ Torr}$ case) [Fig. 6(a)]. The DCDF can be approximated by the Gaussian distribution with the variance shown in Fig. 6(b). As in the $P = 0.3 \text{ Torr}$ case [Fig. 5(d)], at late afterglow times, there is some difference between the DCDF and F_{Gk} for $P = 0.9 \text{ Torr}$ [Fig. 6(a)].

σ_z^2 decreases with increasing time, until $t \leq 10 \text{ ms}$ because of decreasing $|Z_d|$. For $10 \text{ ms} < t \leq 30 \text{ ms}$, the variance increases with increasing t because the ion flux to a dust particle is larger than the

one of electrons ($\nu_{id} > \nu_{ed}$). For $t > 5 \text{ ms}$, σ_z^2 obtained in the $\gamma_m = 0.1$ case is larger than the variance calculated at $\gamma_m = 0$. These time-dependencies are similar to the ones calculated for the fast transition [Fig. 3(d)].

IV. CONCLUSIONS

Thus, the DCDFs in an afterglow plasma were obtained from the master equation [Eq. (5)] for different afterglow times and were compared with those measured in experiments³⁶ for pressures $P = 0.3 \text{ Torr}$ and $P = 0.9 \text{ Torr}$. The DCDFs were found to be in a good qualitative agreement, if the dust discharging model accounts for the emission of electrons in the collisions of argon atoms in excited states with dust particles. The calculated DCDFs at different afterglow times also appeared to be well approximated by Gaussian distributions with the variances described by Eq. (8) as proposed in Refs. 32 and 34. However, at late afterglow times, the Gaussian distributions may be slightly different from those obtained from Eq. (5) [Figs. 3(c), 5(d), and 6(a)]. The difference is due to the fact that the Gaussian distributions were obtained assuming that the variance is smaller than Z_d^2 (see Refs. 32 and 34), which is not the case in the late afterglow for the conditions here (Figs. 3 and 6). We also obtained the time-dependencies for mean dust charge Z_d assuming that the charge changes continuously in the afterglow plasma [Figs. 2(a) and 5(a)]. The time-dependencies for Z_d are almost the same as those for the charge $Z_{d\text{max}}^k$ corresponding to the maximum of DCDF. The variance of the dust charge as a function of time was also obtained for different conditions.

The study was carried out using a spatially averaged model, which accounts for the transition from ambipolar to free diffusion in the afterglow plasma. The cases of fast transition and slow transition were considered, nearly in the same way as in Ref. 36. Meantime, the dust discharging model presented here has some advantages compared with the model in Ref. 36. In particular, our model accounts for the effect of metastable-dust collisions on the DCDF. The results presented here show that these collisions may affect essentially the mean dust charge, the DCDF and the variance at late afterglow times. These processes play a role even if the secondary emission yield, characterizing the electron emission from dust surface at collisions of dust particles with argon atoms in excited states, is small (≤ 0.1).³⁸

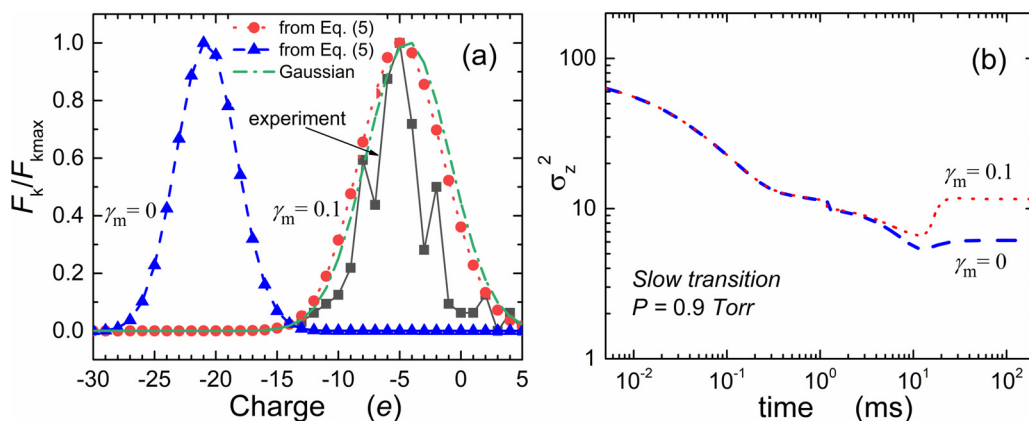


FIG. 6. The normalized calculated dust charge distribution function (a) and the variance (b) for $\gamma_m = 0$ (dashed curve) and 0.1 (dotted curve), and the normalized DCDF (a) obtained in experiments³⁶ (solid curve). In Fig. 6(a), the dashed and dotted curves correspond to the DCDF obtained from Eq. (5), while the dash-dotted curve corresponds to F_{Gk} (for $\gamma_m = 0.1$). Here, $P = 0.9 \text{ Torr}$ and the other conditions are the same as in Fig. 5.

Moreover, our model accounts for multistep ionization and excitation and deexcitation of argon atoms in the electron power balance in the plasma afterglow. The last processes may significantly affect the time-dependence of electron temperature and, as a consequence, other plasma parameters (see the [supplementary material](#)).

However, the model here has some limitations. First, we did not calculate plasma parameters as functions of spatial coordinates. The dependencies for the electron and ion diffusion coefficients on the electron Debye length are taken from Refs. 42–45, which were obtained empirically analyzing different experimental, theoretical and numerical results. Moreover, we cannot determine which regime, fast transition or slow transition, is realized for the conditions here. We expect that after development of 1D or 2D models for afterglow dusty plasmas, it will be possible to describe more correctly the ion and electron diffusion in the plasma afterglow. These models should allow to determine the location of dust particles in plasma volume and to find the dust charge distribution function and other plasma parameters as functions of spatial coordinates. Including the effects of spatial inhomogeneity should also allow to analyze the time-variation of sheaths and voids in afterglow dusty plasmas. Second, we assumed that the electron energy distribution function is Maxwellian during the whole afterglow period. In reality, the EEDF in rf plasmas can differ essentially from the Maxwellian distribution,⁵⁰ and its shape changes with time in afterglow plasmas.⁵⁷ Moreover, the real values of γ_m for the conditions here are not known. In our simulations, the secondary emission coefficients are taken to fit the results of simulations to experimental data. In reality, the value of γ_m is a function of dust size, dust material and the value E/n_a , where E is the electric field,^{13,38} i.e., γ_m depends on neutral gas pressure ($n_a \sim P$). We also did not account in our model for the secondary emission induced by ion–dust collisions. The results of our calculations (shown in [supplementary material](#)) revealed that this process does not affect essentially the mean dust charge, dust charge distribution function and plasma parameters in the plasma afterglow for typical values of the yield (≤ 0.1)^{16,38} characterizing the electron emission from dust surface at collisions of dust particles with ions. The effect of this process on dust charge and DCDF is less important than that of the secondary emission induced by collisions of metastable atoms with dust particles because the ion density decreases faster in the plasma afterglow than the density of metastable atoms (Figs. 2 and 5).

Note that the results here are obtained for the case when the dust particles in the plasma have the same size. Therefore, our results can be used only to analyze experiments, in which the particles grow nearly monodisperse, i.e., their size distribution is very narrow.^{58,59} However, in many experiments on dusty plasma, the plasma may contain dust particles of different radius.^{60,61} The model here allows to find how dust charge characteristics depend on dust radius (see the [supplementary material](#)). The preliminary results of the study of dust radius effects showed that the mean dust charge, the dust charge distribution function, and the variance depend strongly on dust radius (see the [supplementary material](#)).

Afterglow properties may also be affected by the electron emission at collisions of plasma species with the walls. However, studies of cold-cathode discharges in argon showed that the yield of the electron emission at collisions of metastable atoms with the walls γ_{wm} is very low if E/n_a is small (≤ 100 Td) (Figs. 9 and 12 in Ref. 38). In afterglow plasmas, the electric fields near plasma walls are usually small, and

therefore, we expect that this emission process is not intensive. Moreover, we expect that γ_{wm} is essentially smaller than the yield γ_m , describing the electron emission at collisions of metastable atoms with dust particles, because the electron affinity of nanosized materials is usually significantly reduced compared to the bulk material affinity.¹³ The electron emission in collisions of argon atoms in the ground state with the walls may also affect plasma properties. However, this process is intensive only if the atom energies are large [>500 eV for “clean” metal surfaces [Fig. 2 and Eq. (B12) from Ref. 38] and >32 eV for “dirty” metal surfaces [Eq. (B17) from Ref. 38]. To the best of our knowledge, the energies of neutral species in afterglow plasmas are usually much smaller than 32 eV.

The model also does not describe the case when the afterglow plasma contains negative ions^{62,63} and different chemically active species, like in Ar/C₂H₂ plasma, widely used for formation of carbonaceous nanoparticles.^{64,65} Moreover, following Ref. 36, we considered here only the case when the dust charge density in the beginning of afterglow is smaller than the electron density ($|n_d Z_d| \ll n_e$). The extension of our studies to the case of large dust charge densities ($|n_d Z_d| \geq n_e$) is planned in our future works.

Note also that in a dusty plasma, as in other plasma systems, different instabilities and wave propagation may be observed at certain conditions.^{1,2,11,66,67} However, in experiments in Ref. 36, it was not reported about an essential effect of oscillations on the properties of afterglow dusty plasma. Moreover, at high pressure (≥ 300 mTorr) considered here, the random fluctuations of the discharge and dust particles can be suppressed.⁶⁷ Therefore, we do not account here for effects of the plasma and dust particle oscillations on afterglow properties.

Thus, the results presented here can be used for qualitative analysis of dust discharging in non-reactive afterglow plasmas and be a base for building more complicated models including the processes not considered in the present study. The model and results presented here can also be useful for benchmarking or verifying experiments and numerical simulations, particularly in non-stationary plasmas containing dust particles. Our future works will be focused on the development of more advanced models of the afterglow dusty plasma, which will include the effects of the non-Maxwellian electron distribution function, spatial nonuniformity of the afterglow, chemical processes in the plasma and will describe the case when the plasma contains negative ions. Moreover, experimental and numerical studies on determination of the correct electron emission yields are also planned.

SUPPLEMENTARY MATERIAL

See the [supplementary material](#) with the results on the effects of multistep ionization and excitation and deexcitation of argon atoms by electron impact on the electron temperature and other parameters of the afterglow plasma, and on the effects of the electron emission at ion–dust collisions. The [supplementary material](#) also contains information on the dependence of dust charge characteristics on dust radius.

AUTHOR DECLARATIONS

Conflict of Interest

The authors have no conflicts to disclose.

Author Contributions

Igor Borysovych Denysenko: Conceptualization (equal); Investigation (equal); Writing – original draft (equal); Writing – review & editing (equal). **Maxime Mikikian:** Conceptualization (equal); Investigation (equal); Writing – original draft (equal); Writing – review & editing (equal). **Nikolai Azarenkov:** Conceptualization (equal); Investigation (equal); Writing – original draft (equal); Writing – review & editing (equal).

DATA AVAILABILITY

The data that support the findings of this study are available within the article and its [supplementary material](#).

REFERENCES

- ¹S. V. Vladimirov and K. Ostrikov, *Phys. Rep.* **393**, 175 (2004).
- ²V. E. Fortov, A. V. Ivlev, S. A. Khrapak, A. G. Khrapak, and G. E. Morfill, *Phys. Rep.* **421**, 1 (2005).
- ³M. Bonitz, C. Henning, and D. Block, *Rep. Prog. Phys.* **73**, 066501 (2010).
- ⁴B. van Minderhout, J. C. A. van Huijstee, R. M. H. Rompelberg, A. Post, A. T. A. Peijnenburg, P. Blom, and J. Beckers, *Nat. Commun.* **12**, 4692 (2021).
- ⁵Z. Haralson and J. Goree, *Phys. Rev. Lett.* **118**, 195001 (2017).
- ⁶*Dusty Plasmas: Physics, Chemistry, and Technological Impacts in Plasma Processing*, edited by A. Bouchoule (Wiley, New York, 1999).
- ⁷L. Boufendi, M. Ch. Jouanny, E. Kovacevic, J. Berndt, and M. Mikikian, *J. Phys. D* **44**, 174035 (2011).
- ⁸H. Kersten, H. Deutsch, E. Stoffels, W. W. Stoffels, G. M. W. Kroesen, and R. Hippler, *Contrib. Plasma Phys.* **41**, 598 (2001).
- ⁹I. Levchenko, M. Keidar, U. Cvelbar, D. Mariotti, A. Mai-Prochnow, J. Fang, and K. Ostrikov, *J. Phys. D* **49**, 273001 (2016).
- ¹⁰J. Winter, *Phys. Plasmas* **7**, 3862 (2000).
- ¹¹M. Pustynnik, A. Pikalev, A. Zobnin, I. Semenov, H. Thomas, and O. Petrov, *Contrib. Plasma Phys.* **61**, e202100126 (2021).
- ¹²M. Mikikian and L. Boufendi, *Phys. Plasmas* **11**, 3733 (2004).
- ¹³U. Kortshagen and U. Bhandarkar, *Phys. Rev. E* **60**, 887 (1999); and references therein.
- ¹⁴J. Goree, *Plasma Sources Sci. Technol.* **3**, 400 (1994).
- ¹⁵A. Michau, P. Swaminathan, S. Longo, and K. Hassouni, *Plasma Phys. Controlled Fusion* **62**, 014002 (2020).
- ¹⁶I. Stefanović, J. Berndt, D. Marić, V. Samara, M. Radmilović-Radjenović, Z. Lj. Petrović, E. Kovacevic, and J. Winter, *Phys. Rev. E* **74**, 026406 (2006).
- ¹⁷I. Denysenko, I. Stefanović, B. Sikimić, J. Winter, N. A. Azarenkov, and N. Sadeghi, *J. Phys. D* **44**, 205204 (2011).
- ¹⁸M. A. Childs and A. Gallagher, *J. Appl. Phys.* **87**, 1086 (2000).
- ¹⁹A. V. Ivlev, M. Kretschmer, M. Zuzic, G. E. Morfill, H. Rothermel, H. M. Thomas, V. E. Fortov, V. I. Molotkov, A. P. Nefedov, A. M. Lipaev, O. F. Petrov, Yu. M. Baturin, A. I. Ivanov, and J. Goree, *Phys. Rev. Lett.* **90**, 055003 (2003).
- ²⁰L. Wörner, A. V. Ivlev, L. Couëdel, P. Huber, M. Schwabe, T. Hagl, M. Mikikian, L. Boufendi, A. Skvortsov, A. M. Lipaev, V. I. Molotkov, O. F. Petrov, V. E. Fortov, H. M. Thomas, and G. E. Morfill, *Phys. Plasmas* **20**, 123702 (2013).
- ²¹N. Chaubey, J. Goree, S. J. Lanham, and M. J. Kushner, *Phys. Plasmas* **28**, 103702 (2021).
- ²²L. Couëdel, M. Mikikian, L. Boufendi, and A. A. Samarian, *Phys. Rev. E* **74**, 026403 (2006).
- ²³I. B. Denysenko, I. Stefanović, B. Sikimić, J. Winter, and N. A. Azarenkov, *Phys. Rev. E* **88**, 023104 (2013).
- ²⁴J. Berndt, E. Kovacevic, V. Selenin, I. Stefanović, and J. Winter, *Plasma Sources Sci. Technol.* **15**, 18 (2006).
- ²⁵I. B. Denysenko, I. Stefanović, M. Mikikian, E. Kovacevic, and J. Berndt, *J. Phys. D* **54**, 065202 (2021).
- ²⁶B. van Minderhout, T. Peijnenburg, P. Blom, J. M. Vogels, G. M. W. Kroesen, and J. Beckers, *J. Phys. D* **52**, 32LT03 (2019).
- ²⁷C. Cui and J. Goree, *IEEE Trans. Plasma Sci.* **22**, 151 (1994).
- ²⁸G. E. Morfill, V. N. Tsytovich, and H. Thomas, *Plasma Phys. Rep.* **29**, 1–30 (2003).
- ²⁹N. G. Van Kampen, *Stochastic Processes in Physics and Chemistry* (Elsevier Science Publishers, North Holland, Amsterdam, 2007).
- ³⁰T. Matsoukas and M. Russell, *J. Appl. Phys.* **77**, 4285 (1995).
- ³¹T. Matsoukas, M. Russell, and M. Smith, *J. Vac. Sci. Technol. A* **14**, 624 (1996).
- ³²B. Shotorban, *Phys. Rev. E* **83**, 066403 (2011).
- ³³S. A. Khrapak, A. P. Nefedov, O. F. Petrov, and O. S. Vaulina, *Phys. Rev. E* **59**, 6017 (1999).
- ³⁴B. Shotorban, *Phys. Plasmas* **21**, 033702 (2014).
- ³⁵L. Couëdel, A. A. Samarian, M. Mikikian, and L. Boufendi, *Europhys. Lett.* **84**, 35002 (2008).
- ³⁶L. Couëdel, A. A. Samarian, M. Mikikian, and L. Boufendi, *Phys. Plasmas* **15**, 063705 (2008).
- ³⁷S. A. Khrapak, S. V. Ratynskaia, A. V. Zobnin, A. D. Usachev, V. V. Yaroshenko, M. H. Thoma, M. Kretschmer, H. Hofner, G. E. Morfill, O. F. Petrov, and V. E. Fortov, *Phys. Rev. E* **72**, 016406 (2005).
- ³⁸A. V. Phelps and Z. L. Petrovic, *Plasma Sources Sci. Technol.* **8**, R21 (1999).
- ³⁹M. A. Ali and P. M. Stone, *Int. J. Mass Spectrom.* **271**, 51 (2008).
- ⁴⁰H. Deutsch, K. Becker, A. N. Grum-Grzhimailo, K. Bartschat, H. Summers, M. Probst, S. Matt-Leubner, and T. D. Märk, *Int. J. Mass Spectrom.* **233**, 39 (2004).
- ⁴¹E. G. Thorsteinsson and J. T. Gudmundsson, *J. Phys. D* **43**, 115201 (2010).
- ⁴²R. A. Gerber and J. B. Gerardo, *Phys. Rev. A* **7**, 781 (1973).
- ⁴³R. J. Freiberg and L. A. Weaver, *Phys. Rev.* **170**, 336 (1968).
- ⁴⁴A. V. Phelps, *J. Res. Natl. Inst. Stand. Technol.* **95**, 407 (1990); and references therein.
- ⁴⁵P. J. Chantry, *J. Appl. Phys.* **62**, 1141 (1987).
- ⁴⁶A. Yanguas-Gil, J. Cotrino, and L. Alves, *J. Phys. D* **38**, 1588 (2005).
- ⁴⁷A. A. Mityureva and V. V. Smirnov, *Opt. Spektrosk.* **97**, 508 (2004).
- ⁴⁸D. P. Lymberopoulos and D. J. Economou, *J. Appl. Phys.* **73**, 3668 (1993).
- ⁴⁹A. Bogaerts, R. Gijbels, and J. Vlcek, *J. Appl. Phys.* **84**, 121 (1998).
- ⁵⁰M. A. Lieberman and A. J. Lichtenberg, *Principle of Plasma Discharges and Material Processing* (Wiley, New York, 2005).
- ⁵¹D. Trunec, P. Španěl, and D. Smith, *Contrib. Plasma Phys.* **34**, 69 (1994).
- ⁵²O. V. Proshina, T. V. Rakhimova, A. S. Kovalev, A. N. Vasilieva, A. I. Zotovich, S. M. Zyryanov, and A. T. Rakhimov, *Plasma Sources Sci. Technol.* **29**, 015015 (2020).
- ⁵³S. Gorchakov, D. Loffhagen, and D. Uhrlandt, *Phys. Rev. E* **74**, 066401 (2006).
- ⁵⁴G. D. Byrne and S. Thompson, see <http://www.radford.edu/~thompson/vodef90web> for “VODE_F90 Support Page,” (2013).
- ⁵⁵A. P. Nefedov, G. E. Morfill, V. E. Fortov, H. M. Thomas, H. Rothermel, T. Hagl, A. V. Ivlev, M. Zuzic, B. A. Klumov, A. M. Lipaev, V. I. Molotkov, O. F. Petrov, Y. P. Gidzenko, S. K. Krikalev, W. Shepherd, A. I. Ivanov, M. Roth, H. Binnenbruck, J. A. Goree, and Y. P. Semenov, *New J. Phys.* **5**, 33 (2003).
- ⁵⁶I. B. Denysenko, M. Mikikian, and N. A. Azarenkov, *J. Phys. D* **55**, 095201 (2022).
- ⁵⁷I. B. Denysenko, H. Kersten, and N. A. Azarenkov, *Phys. Plasmas* **23**, 053704 (2016).
- ⁵⁸I. Denysenko, J. Berndt, E. Kovacevic, I. Stefanovic, V. Selenin, and J. Winter, *Phys. Plasmas* **13**, 073507 (2006).
- ⁵⁹A. M. Hinz, E. von Wahl, F. Faupel, T. Strunskus, and H. Kersten, *J. Phys. D* **48**, 055203 (2015).
- ⁶⁰F. Greiner, A. Melzer, B. Tadsen, S. Groth, C. Killer, F. Kirchschrager, F. Wiebl, A. Pilch, H. Krüger, D. Block, A. Piel, and S. Wolf, *Eur. Phys. J. D* **72**, 81 (2018).
- ⁶¹P. K. Shukla and B. Eliasson, *Rev. Mod. Phys.* **81**, 25 (2009).
- ⁶²I. Kaganovich, *Phys. Plasmas* **8**, 2540 (2001).
- ⁶³I. D. Kaganovich, B. N. Ramamurthi, and D. J. Economou, *Phys. Rev. E* **64**, 036402 (2001).
- ⁶⁴I. B. Denysenko, E. von Wahl, S. Labidi, M. Mikikian, H. Kersten, T. Gibert, E. Kovačević, and N. A. Azarenkov, *Plasma Phys. Controlled Fusion* **61**, 014014 (2019).
- ⁶⁵G. Tetard, A. Michau, S. Prasanna, J. Mougenot, P. Brault, and K. Hassouni, *Plasma Sources Sci. Technol.* **30**, 105015 (2021).
- ⁶⁶V. Nosenko, J. Goree, and A. Piel, *Phys. Rev. Lett.* **97**, 115001 (2006).
- ⁶⁷J. H. Chu, J. B. Du, and I. Lin, *J. Phys. D* **27**, 296 (1994).